High Performance Room Temperature Rectenna IR Detectors Using Graphene Geometric Diodes

Zixu Zhu, *Student Member, IEEE*, Saumil Joshi, *Student Member, IEEE*, and Garret Moddel, *Senior Member, IEEE*

***Abstract*—High performance rectenna detectors that operate at room temperature have been developed for the frequency range of terahertz to infrared (IR). We formed IR rectennas by coupling bowtie antennas to ultrafast diodes, called geometric diodes. Geometric diodes rely on geometric asymmetry and the long charge carrier mean-free path length of graphene to provide asymmetric current-voltage characteristics. The planar structure of the geometric diode provides the femtosecond RC time constant necessary for detection of IR frequencies. Fabricated IR rectennas using graphene geometric diodes have shown strong optical response to 28 THz CO_2 laser illumination at room temperature. The detectivity (D^*) and the noise equivalent power (NEP) of the IR rectennas are calculated to be on the order of 10^8 cm $Hz^{1/2}W^{-1}$ and 10^{-9} W $Hz^{-1/2}$, respectively. Simulations show that with some improvement room temperature rectennas using graphene geometric diodes are able to achieve an NEP value as low as 10^{-11} W $Hz^{-1/2}$.**

***Index Terms*—Detector, diode, graphene, infrared (IR), NEP, rectenna, room temperature, terahertz.**

I. Introduction and Background

CONVENTIONAL infrared (IR) detectors and terahertz detectors are classified into two types, thermal detectors and photon detectors [1]. Neither type of IR detector has dominated the market because they each have their own limitations. Low frame rates limit thermal IR detectors while the need for cryogenic cooling limits photon IR detectors. We have successfully demonstrated a room temperature, high performance IR rectenna detector that does not belong to either thermal or photon detector categories and does not suffer from their limitations.

The development of IR detectors started with thermal detectors, which can be traced back to Herschel's experiment with thermometers about 200 years ago [2] and Langley's bolometer in 1880 [3]. Thermal detectors absorb the incident radiation to change the temperature of the material within detectors. This results in a change in their electrical properties. For example, the resistance of a bolometer changes with temperature. The magnitude of the change is proportional to the incident radiation power. Thermal detectors are able to work at room temperature and normally require a heat sink. Their detection performance is generally wavelength independent, but the response is relatively slow compared to photon detectors [1], [4].

Manuscript received February 1, 2014; revised April 2, 2014; accepted April 10, 2014. This work was supported by Abengoa Solar and the Center for Revolutionary Solar Photoconversion, with initial support from Hub Lab.

The authors are with the Department of Electrical Engineering, University of Colorado, Boulder, CO 80309 USA (e-mail: zixu.zhu@colorado.edu; saumil.joshi@colorado.edu; moddel@colorado.edu).

Color versions of one or more of the figures in this paper are available online at http://ieeexplore.ieee.org.

Digital Object Identifier 10.1109/JSTQE.2014.2318276

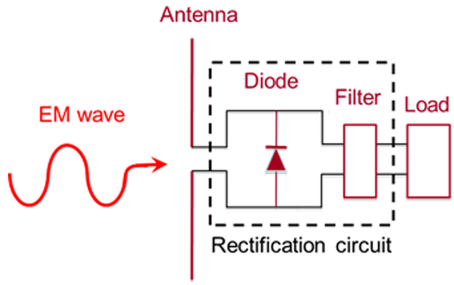

Fig. 1. Schematic diagram of a rectenna. An incident EM wave is received by the antenna, and rectified by the circuit containing a high speed diode and a low pass filter, providing a dc output to the load. This figure is from ref [7].

The development of photon detectors relates closely to the development of semiconductor technology. The first IR photoconductor was invented by Case in 1917 [5]. Sixteen years later, Kutzscher discovered that lead sulphide was photoconductive and could be used as a photon detector for a wavelength of 3 μm [6]. The electrical output of a photon detector is the photocurrent generated due to the absorption of a photon by the semiconductor material. Since the absorbed photon energy has to be larger than the bandgap energy of the semiconductor material, photon detectors are wavelength dependent. Photon detectors usually respond much faster than thermal detectors. However, IR photons and terahertz photons have much lower energy than photons at visible frequencies, and therefore IR and terahertz photon detectors require cryogenic cooling to achieve good signal-to-noise performance to keep the thermally generated current below the level of the photocurrent. IR systems based on semiconductor photon detectors are normally expensive, heavy, and inconvenient to use [1].

II. Principle of Operation

A. Rectenna Detector

Rectenna IR and terahertz detectors can be considered ultrahigh frequency radio receivers. Fig. 1 shows the configuration of a rectenna system. Rectennas have two main components: antennas and diodes. The function of the antenna is to absorb radiation in its electromagnetic (EM) form and convert it into an ac current input to the diode. The ultrafast diode rectifies the ac to provide a dc output to the load. Rectenna detectors have fast responses and do not require cryogenic cooling. They are sensitive to the polarization of the incident radiation and can be either wavelength selective or broadband depending on the antenna design.

Extensive research has been carried out on high efficiency IR antennas [8]. The bottleneck for terahertz and IR rectenna technology lies in the diodes. The two primary requirements for

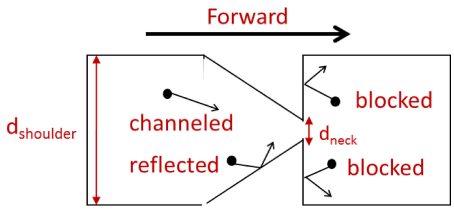

Fig. 2. The structure of an inverse arrowhead geometric diode. The width of the neck (d_{neck}) is on the order of the charge carrier MFPL in the material. Charge carriers reflect off the interior boundaries of the diode. We call the inverse arrowhead direction from left to right the forward direction for carrier transport. On the left side of the neck charge carriers can either channel directly through the neck region, or reflect at the tapering edge and have a chance to keep moving forward. On the right side of the neck the vertical edge blocks the majority of the charges. This figure is from ref [7].

a working rectenna diode are high operating speed and a good impedance match to the antenna. For the diode to be sufficiently fast it must respond to the terahertz signal intrinsically, and also the RC time constant of the circuit consisting of both the diode and the antenna must be shorter than the period of the incident wave. Conventional semiconductor diodes, such as p-n junction diodes and Schottky diodes, cannot rectify IR frequencies, and with few exceptions, terahertz. The most widely investigated diode for terahertz rectennas is the metal-insulator-metal (MIM) diode. Parallel plate MIM devices suffer from fundamental RC constraints [9]. As a result, MIM diode operation beyond a few terahertz is inefficient.

B. Geometric Diode

We proposed a new type of ultra-fast diode, called a geometric diode [10], and demonstrated its operation at dc [11], and at 28 THz [7]. Rectenna detectors using geometric diodes have the potential to revolutionize the field of IR and terahertz detectors.

Geometric diodes are locally ballistic transport devices, where the critical dimension of the device is on the order of charge mean-free path length (MFPL) of the material [10]. They rely on the device's physical asymmetry to achieve diode behavior. Dragoman used a quantum approach to simulate similar structures [12], and demonstrated the device dc electrical characteristics [13]. Semiconductor devices relying on geometric asymmetry were demonstrated by A. M Song [14]. The devices took the advantage of the geometric effect in a patterned gallium arsenide film and used hot electrons as charge carriers to function as a full-wave rectifier.

The principle of operation of the geometric diode exploits an asymmetric device geometry to control charge carrier movement. In Fig. 2, we show a schematic diagram of one form of the geometric diode. A conductive thin film is patterned into an inverse arrowhead shape. The width of the constricted neck region at the end of the arrowhead is on the order of charge carrier MFPL in the material. The shape of such a ballistic device influences the charge carrier transport within the geometric diode. Charges are reflected at the boundaries of the sloped arrowhead and can funnel from left to right (forward direction) through the neck. Conversely, the vertical sidewall of the arrowhead blocks the charges moving from right to left (reverse). Thus, the inverse arrowhead shape of the diode determines the preferred forward direction for charge flow to be from left to right. At zero bias, charge transport will achieve equilibrium and create a built-in voltage due to the gradient of the charge concentration caused by the geometric effect, resulting in zero net current. Under bias, charges face less resistance in the forward direction than in the reverse direction. Such a geometric effect leads to a current–voltage [*I(V)*] asymmetry, and the device behaves as a diode. To obtain a large geometric effect, the carrier MFPL in the thin film material has to be sufficiently large compared to the neck width. Therefore, we chose graphene as the material for its long MFPL [15].

Unlike semiconductor diodes, which are transit time limited, and conventional MIM diodes, which are RC time constant limited [9], geometric diodes are exceptional candidates for IR and terahertz rectenna detectors. Geometric diodes are formed from patterned conductive thin films. Therefore, by varying the geometry their impedance can be adjusted for a good match with the antennas. As for the intrinsic speed, graphene is capable of operating at terahertz frequencies [16]–[18]. High quality graphene samples support plasmon waves that are weakly damped [19], [20] with a gate-tunable surface plasmon frequency [21] up to the graphene optical phonon frequency of 48.3 THz [22]. More importantly, geometric diodes have ultra-low capacitance. Based on a planar film capacitance model, we estimate the capacitance of an arrowhead shaped geometric diode with a 100 nm neck width to be between 10^{-17} and 10^{-18} F [7]. Since the impedance of antennas is normally about 100 Ω the RC time constant of an impedance matched rectenna system using graphene geometric diodes is on the order of 10^{-15} s. Thus in theory, geometric diodes do not suffer from RC constraints up to approximately 100 THz, and we have measured their response at 28 THz.

III. Simulation of Geometric Diodes

Monte Carlo simulations based on the Drude model [23] have been used to model the transport of charges within the device [11]. In the Monte Carlo simulation, charges move ballistically between collisions within the structure and reflect specularly at the edges of the device. Their velocities are the sum of the drift velocity and a randomly directed Fermi velocity, which is regenerated in magnitude and direction after every collision. The drift velocity is calculated from the electric field due to the applied drain-source voltage, and the effective mass of the electrons in the material [24]. Although only a few collisions were needed for an electron to move from the left edge of the device to the right edge of the device, the electrons looped through the device enough times to undergo 10^6 collisions ($\sim 10^3$–10^5 loops), which was required to achieve stable and low noise *I(V)* curves. The simulated results in Fig. 3 show that increasing the charge MFPL and reducing neck width (d_{neck}) increases the asymmetry of the diode *I(V)* curve. Detailed Monte-Carlo simulation results for geometric diodes can be found in references [11] and [7].

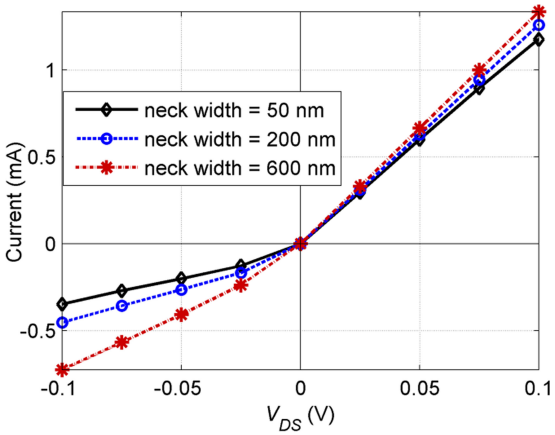

Fig. 3. Simulated *I(V)* curves for a geometric diode with different neck widths (d_{neck}) and a fixed shoulder width $(d_{\mathrm{shoulder}}$ as shown in Fig. 2) of 1 μm. The MPFL is set to be 200 nm in all the simulations. Narrower necks restrict the reverse current more effectively. This figure is from ref [7].

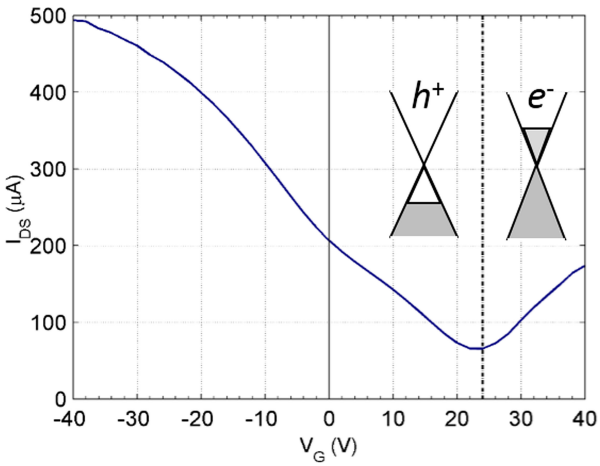

Fig. 4. Dirac curve [drain-source current (I_{DS}) versus back gate voltage (V_G)] of the graphene used for fabricating the graphene geometric diode. The drain-source voltage V_{DS} was fixed at 1.5 V. The CNP voltage (V_{CNP}) is 24 V. When V_G is less than V_{CNP}, the majority charge carriers within graphene are holes (h^+). When V_G is larger than V_{CNP}, the charge carriers are electrons (e^-). This figure is from ref [7].

IV. Fabricated Devices and Measurement Results

A. Material for Geometric Diodes—Graphene

We choose graphene as the material for its long charge MFPL and capability of handling extremely high current density, $\sim 10^8\,\mathrm{A/cm^2}$. This allows for devices that are sufficiently large to be fabricated within the capabilities of current lithography techniques. The MFPL of graphene is long, due to its unique atomic structure and high electron mobility [15]. Research groups have reported electron MFPLs in graphene up to a few micrometers [25], [26]. The MFPL can be calculated from a measurement of the drain-source current (I_{DS}) versus gate voltage (V_G), sometimes called the Dirac curve [15]. Fig. 4 shows the Dirac curve of our graphene prepared using the exfoliation method. The gate voltage (V_G) at which the device has a minimum drain source current (I_{DS}) is the charge neutral point (CNP) voltage (V_{CNP}). At this voltage, the electron and hole concentrations are the same and conductivity of graphene reduces to a minimum. The CNP voltage V_{CNP} of the graphene used in this study is 24 V. The backscattering MFPL was calculated to be 45 nm [27]. The charge carrier concentration in the simulation is determined to be $1.1 \times 10^{12}\,\mathrm{cm^{-2}}$ at a gate voltage of 30 V, 6 V away from the V_{CNP}.

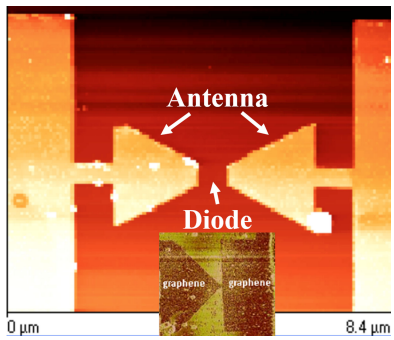

Fig. 5. AFM image of a rectenna detector. In the rectenna, a graphene geometric diode couples to a metal bowtie antenna. Compared to the thickness of graphene, the significantly thicker metal antenna results in a low contrast between graphene and the SiO_2 substrate, and therefore the graphene is not visible in this AFM image. The inset shows the AFM image of a geometric diode similar to the diode located at the center of the antenna gap region. This figure is from ref [7].

B. Fabrication Method

We used exfoliation to produce graphene flakes on 90 nm thermally grown SiO_2 silicon wafer substrates [15]. The geometric diodes were patterned using electron-beam (e-beam) lithography followed by an oxygen plasma etch. We used maN negative resist and a JEOL 9300 electron beam writer for the e-beam patterning process. An Oxford PlasmaLab 80+ RIE system with an oxygen plasma power of 50 W was used for 12 s to etch the graphene. The diodes were fabricated with a four-point probe configuration to remove the contact resistance from the measurement [7]. Four metal contacts (15 nm Cr/40 nm Au) were thermally evaporated and lifted off using resist patterned by photolithography.

C. Fabricated Geometric Diodes With Antennas

The 28 THz IR rectenna detectors were fabricated with 5.1 μm long metal bowtie antennas and graphene geometric diodes configured in an edge-fed arrangement [28], as shown in Fig. 5. The antenna is a combination of two opposing 2.3 μm long triangular metal sections (15 nm/45 nm thermally evaporated Cr/Au). It is coupled to a 500 nm long graphene geometric diode placed at the center of the antenna gap region. The neck width of the diode is approximately 75 nm, measured with an atomic force microscope (AFM).

D. Diode DC I(V) Measurement

Before performing the optical response measurements of the rectenna detectors, the *I(V)* characteristics of graphene geometric diodes were measured at dc. Four-point measurements with pulsed bias voltage were carried out to eliminate the contact resistance [7]. The four-point measurement setup is

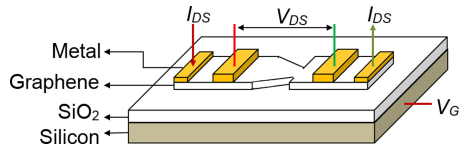

Fig. 6. Four-point probe measurement setup circumvents contact resistance that distorts two-point measurements. A pulsed voltage was applied to provide drain-source current ($I_{\rm DS}$) through the outer two metal contacts. The actual voltage drop across the diode ($V_{\rm DS}$) was measured between the inner metal contacts. A back gate voltage (V_G) was applied directly to the silicon substrate to control the carrier type and concentration in the graphene. This figure is from ref [30].

shown in Fig. 6. Channel A of a Keithley 2612 Sourcemeter was used to provide the pulsed dc voltage at the outer two contacts and the current $I_{\rm DS}$ was measured at the same time. By configuring the same channel of the Sourcemeter to be in "4-Wire" mode, we were able to measure the actual voltage drop $V_{\rm DS}$ across the diode between the inner two contacts. In the gate effect measurement, Channel B of the same Sourcemeter was used to apply a back gate voltage V_G to the silicon substrate. At room temperature and atmosphere environment, graphene electronic devices suffer from hysteresis effect [29]. To achieve accurate *I(V)* characteristics, the applied dc voltage was pulsed with a pulse width of 26 μs and followed this pattern: $0V, +V_1, -V_1, +V_2, -V_2, ... + V_{\rm end}, -V_{\rm end}$.

The graphene geometric diode exhibited a nonlinear asymmetric *I(V)* relationship, as shown in Fig. 7(a). For IR detector applications, an important figure of merit for the diode is the responsivity, which is defined as one half of the ratio of the second derivative to the first derivative of the *I(V)* $[1/2 \times I''(V)/I'(V)]$. The responsivity represents how much dc current can be generated for a given ac input power. The responsivity of the diode of Fig. 7(a) is plotted in Fig. 7(b). This stand-alone diode has a responsivity of 0.12 A/W at zero bias voltage, and over 0.2 A/W under bias. Due to the inconsistence of the fabrication process of geometric diodes, the performance of fabricated geometric diodes vary among devices. The diode in Fig. 5 has a lower responsivity than the diode in Fig. 7. Its diode responsivity is ~0.03 A/W.

E. Detector Optical Response Measurement

To measure the optical response, we illuminated the rectennas with 28 THz radiation from a CO_2 laser. Two-point measurements were performed on the antenna-coupled diodes in air at room temperature. The optical measurement setup is shown in Fig. 8. A SYNRAD 48–1SWJ IR CO_2 laser generated the 28 THz radiation. The power from the CO_2 laser was controlled by changing the pulse width from a pulse generator. We used a red He-Ne laser to assist in aligning the CO_2 laser to the device. A half-wave plate on the optical path rotated the laser's polarization relative to the antenna axis. A Stanford Research Systems (SRS) chopper with 25 blades was used to mechanically chop the laser beam at 280 Hz. The same chopper produced a reference signal for the SR830 lock-in amplifier, so that the lock-in amplifier was able to detect the modulated output current and voltage signal at the chopping frequency. Before and after every optical measurement, a mercury switch shorted the probes

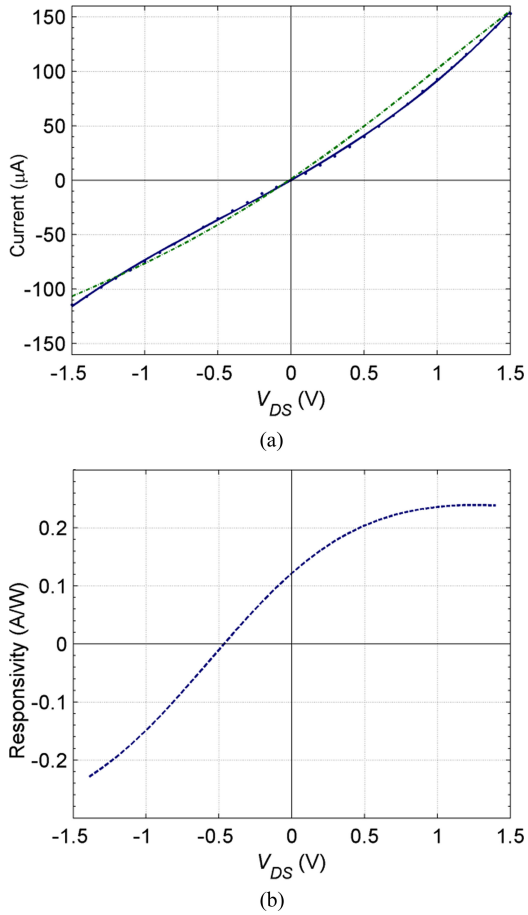

Fig. 7. (a) DC *I(V)* characteristics (solid blue) of an exfoliated graphene geometric diode at a gate voltage of 20 V. The Monte Carlo simulation (dashed green) uses the dimensions of the fabricated device: neck width = 75 nm, shoulder width = 400 nm, and the measured MFPL = 45 nm; (b) Calculated responsivity $[1/2|I''(V)/I'(V)|]$ as a function of the applied drain-source bias. At 0 V bias, the responsivity is 0.12 A/W. This figure is from ref [7].

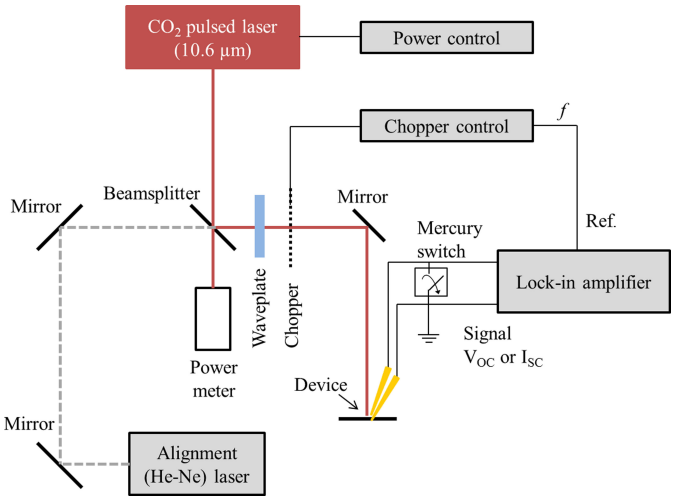

Fig. 8. Optical response measurement setup of the rectenna. We used a red He-Ne laser to align the CO_2 laser. A two-point probe setup was used for measuring the open circuit voltage and short circuit current. The lock-in amplifier used a 280 Hz signal from a chopper as the reference. To study the effect of changing the angle between the antenna axis and the incident wave polarization, a half-wave plate was used. This figure is from ref [7].

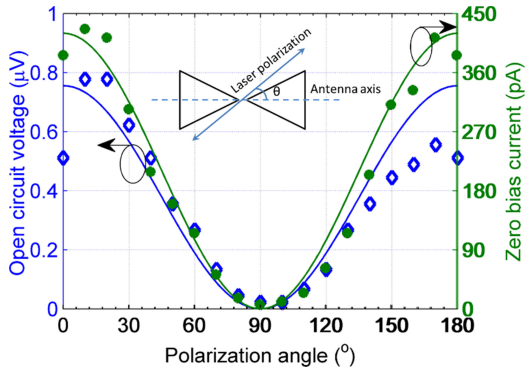

Fig. 9. Metal antenna/graphene diode rectenna short-circuit current (green circles) and open-circuit voltage (blue diamonds) as a function of polarization angle (θ) under CO_2 laser illumination of 49 mW/mm^2.

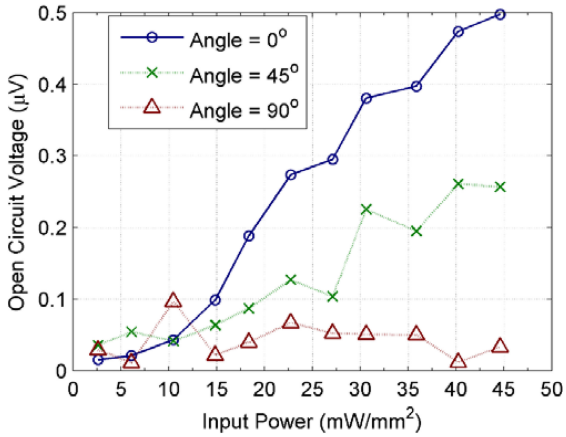

Fig. 10. Open circuit voltage versus laser input intensity at three polarization angles: 0°, 45° and 90°. The response at 0° (blue circles) indicates perfect alignment between the laser polarization and the antenna, which gives the strongest open circuit voltage signal. At 90° (green crosses), the antenna is perpendicular to the laser polarization and gives a near zero output voltage at all input intensities.

to the ground potential to avoid damage to the devices from electrostatic discharge.

Fig. 9 shows the optical response of the rectenna detector under illumination. Although the maximum responsivity occurs at $V_{\rm DS} > 1$V dc bias, as shown in Fig. 7(b), no external $V_{\rm DS}$ was needed during optical measurements because the diode had sufficient asymmetry at zero bias. Both the rectified open-circuit voltage and short-circuit current in Fig. 9 have cosine-squared dependences with the polarization angle, confirming that the optical response was due to the radiation coupled through the bowtie antenna. This angular dependence of the optical response indicates that the rectification was neither caused by diffusion of optically generated charge carriers, nor was a result of thermoelectric effects due to non-uniform illumination of the diode. Additionally, no gate voltage was applied during the measurement, and we discharged the device to the ground through a mercury switch before the measurement. Therefore, no p-n junctions could have been formed as a result of zero $V_{\rm DS}$ and V_G bias [31].

Two additional measurements were performed to confirm that the rectenna responds at 28 THz. First, we illuminated graphene geometric diodes without coupled antennas. As expected, diodes without antennas did not show any optical response. This indicates that the optical response shown in Fig. 9 is not caused by in-situ p-n doping in the graphene [31]. Second, as shown in Fig. 10, the amplitude of the on-axis polarization ($\theta = 0^\circ$) response increases as the incident radiation intensity increases. In contrast, for the misaligned case ($\theta = 90^\circ$) the detector output remains at the noise voltage level regardless of the change in the laser intensity. Thus, the graphene geometric diode genuinely rectifies the 28 THz signal absorbed by the antenna.

In the next two sections, we first verify that our measured detector output is in quantitative agreement with the estimated output. After a short review on the performance of existing IR and terahertz detectors, the figures of merit of those detectors will be compared with those of our IR and terahertz rectenna detectors.

V. Discussion of Measurement Results

To confirm that the measured results at 28 THz are consistent with our model for the device operation, we estimate the output signal of the rectennas based on the measured dc *I(V)* behavior of the geometric diode. When the rectenna axis was aligned with the laser polarization, the short-circuit current output of the rectenna was measured to be 420 pA. In calculating the expected short-circuit current we take into account the following system parameters: measured laser intensity ($P_{\rm in}$), reported antenna absorption efficiency (η_a), measured diode responsivity (β_d), and calculated rectenna coupling efficiency (η_c). We measured the illumination intensity ($P_{\rm in}$) using a Scientech Astral AC25FXS power meter to be 49 mW/mm^2 assuming the device was 1 mm offset from the beam center. The effective area ($A_{\rm eff}$) of the 28 THz metal bowtie antenna with the same configuration is reported to be 37.5 m^2. The measured antenna absorption efficiency is 37% [32]. The antenna impedance (R_a) is assumed to be 100 Ω, which is a typical for an antenna operating at terahertz frequencies [33]. We measured the dc *I(V)* behavior of the diode in the rectenna and calculated its responsivity to be 0.0285 A/W at zero-bias. Based on the *I(V)* data, a diode resistance (R_d) of ~3000 Ω was calculated. As mentioned in the beginning of the paper, the diode capacitance (C_d) was calculated to be $\sim 10^{-18}$ F. Using an impedance matching model [9] in (1), the rectenna coupling efficiency is calculated to be 12%

$$\eta_c = \frac{4\frac{R_a R_d}{(R_a+R_d)^2}}{1+\left(\omega\frac{R_a R_d}{(R_a+R_d)}C_d\right)^2} \tag{1}$$

where ω is the radiation frequency, which is $2\pi \times 28$ THz. The estimated current is

$$I_{\rm est} = P_{\rm in} A_{\rm eff} \eta_a \beta_d \eta_c. \tag{2}$$

Combining all the above parameters and using (2), the metal antenna/graphene geometric diode rectenna gives an estimated current of 2.6 nA, which is greater than the measured current probably because of incorrect estimates of the antenna efficiency and impedance match.

VI. Comparison With Other IR and Terahertz Detectors

To compare the geometric diode rectenna with other detector technologies used in IR imaging and terahertz radiation detection, several detector characteristics need to be considered: system responsivity, normalized detectivity (D^*), noise equivalent power (NEP), working temperature, and imaging frame rate.

We define the rectenna system responsivity ($\beta_{\rm sys}$) in (3) to be the product of the antenna absorption efficiency, the diode responsivity, and the system coupling efficiency. The rectenna system responsivity is the current output of the rectenna system for a given incident optical power

$$\beta_{\rm sys} = \eta_a \beta_d \eta_c. \tag{3}$$

The responsivity of the rectenna detector in Fig. 5 is calculated to be 0.2 mA/W. The normalized detectivity D^* is a measure of the noise performance of the detector and is defined as [8]:

$$D^* = (A_d \Delta f)^{1/2} \frac{\beta_{\rm sys}}{I_n} \tag{4}$$

where

$$I_n = \sqrt{\left(2eI_{\rm bias} + \frac{4KT}{R_d}\right)\Delta f}. \tag{5}$$

For the rectenna system, Δf is the bandwidth of the detector and A_d is the area of the detector, which equals the effective area ($A_{\rm eff}$) of the antenna for rectennas. The noise current (I_n) is calculated as the sum of the shot noise from the diode dc bias current ($I_{\rm bias}$) and the Johnson thermal noise from the diode resistance. Our rectenna detectors work at zero bias ($I_{\rm bias} = 0$ A) and room temperature ($T = 300$ K). D^* is calculated to be 2.6×10^6 cm $\rm Hz^{1/2}W^{-1}$.

Another detector characteristic, the NEP, is a measure of the minimum incident optical power required for unity system signal to noise ratio [34]. A lower NEP value represents better detector sensitivity. NEP is related to D^* and is defined as [7]:

$$\text{NEP} = \frac{\sqrt{A_d}}{D^*}. \tag{6}$$

The NEP of the metal antenna / graphene geometric diode rectenna IR detector is calculated to be 43 nW $\rm Hz^{-1/2}$.

Thermal bolometer IR detectors working at wavelengths of 2 to 40 μm typically have a D^* between 10^8 and 10^{10} cm $\rm Hz^{1/2}W^{-1}$ at 77 K [4] and between 10^6 to 10^8 cm $\rm Hz^{1/2}W^{-1}$ [35] at room temperature. They are capable of operating at room temperature, with a frame rate on the order of a few milliseconds. Our rectenna IR detectors using graphene geometric diodes have a much faster frame rate than thermal IR detectors. The fundamental limit of the frame rate is the circuit RC time constant, which is shorter than 10^{-12} s.

Compared to photon detectors, rectenna IR detectors are able to operate at room temperature and also are sensitive to the polarization of the incoming radiation. Photon detectors based on mercury cadmium telluride (HgCdTe) have become the most widely used IR detector for mid and long wavelength (3–30 μm) IR radiation. The III–V (InGaAs, InAsSb, InGaSb) detectors are used mostly for short wavelength IR. At 77 K and 10.6 μm wavelength, HgCdTe IR detectors have achieved D^* on the order of $10^{10}\,\rm cm\,Hz^{1/2}W^{-1}$ [1]. The D^* of semiconductor photon detectors in general decays by a factor of 10 for every 10 K increase in temperature [4]. A number of concepts [1], [36], [37] have been proposed to improve performance of photon detectors operating at near room temperature. Multijunction HgCdTe photodiodes are capable of achieving a D^* of $10^8\,\rm cmHz^{1/2}W^{-1}$ at 10.6 μm wavelength [36].

At the time of writing of this paper, there are no other graphene detectors for 28 THz detection. When the incident radiation frequency is below the RC limit of the rectenna, the size of the antenna can be adjusted to any frequency. Therefore, we can compare our rectenna to graphene detectors operating at $\sim$1 THz. Tredicucci *et al*. have experimentally demonstrated a graphene field effect transistor (FET) working at 1 THz [18]. In this graphene FET detector, the top gate of a graphene transistor is coupled with one arm of a terahertz metal bowtie antenna while the other arm of the antenna acts as the source terminal of the transistor. The detector responsivity is produced by a second-order nonlinear effect when an oscillating terahertz field is applied between the gate and the source terminals. The dc photovoltage output is proportional to the derivative of the drain-source channel conductivity with respect to the gate voltage. The performance of the graphene FET is fundamentally limited to the graphene top gate capacitance coupling efficiency, which also limits its operating frequency. Our current graphene geometric diode rectenna is at least as good as this graphene FET terahertz detector, which has an NEP of 30 nW $\rm Hz^{-1/2}$ for double layer graphene devices, and 200 nW $\rm Hz^{-1/2}$ for single layer graphene devices.

Rectennas using MIM diodes provide another approach for IR and terahertz detection. Although conventional lumped element MIM diodes are limited in performance by their RC time constant at 28 THz, room temperature rectennas using MIM diodes can achieve high D^* and low NEP at 1 THz. A resistance matched Ni-NiO-Ni MIM diode in a rectenna (100 Ω at 0.33 V with 0.74 mA bias) has a coupling efficiency of 77% and a system responsivity of 5.2 A/W. In theory, the D^* of rectennas working at 1 THz with lumped element Ni-NiO-Ni MIM diodes is 1.89×10^8 cm $\rm Hz^{1/2}W^{-1}$, assuming an antenna area of 0.09 $\rm mm^2$ [30]. Due to the low coupling efficiency of MIM rectenna system at 28 THz, the D^* of the same Ni-NiO-Ni diode rectenna drops to 8.9×10^5 cm $\rm Hz^{1/2}W^{-1}$.

IR rectennas using MIM diodes have been demonstrated by several groups [38], [39]. An impedance matched MIM diode operating at 28 THz requires a diode area of 0.001 $\mu\rm m^2$ with 0.3 nm insulator thickness [40]. Such a diode will provide a theoretical NEP as low as 5 nW $\rm Hz^{-1/2}$ to the rectenna system. IR rectennas using practical MIM diodes have a typical NEP value on the order of 10^{-6} W $\rm Hz^{-1/2}$ [41]. We proposed a potential solution to the RC coupling issue by using rectennas with MIM traveling wave diodes for 28 THz detection [42], [43]. The approach is to fabricate MIM diodes into a traveling wave configuration. The predicted D^* of traveling wave MIM diode rectennas can be as high as 10^9 cm $\rm Hz^{1/2}W^{-1}$.

In Table I, we summarize the performance of the IR and terahertz detectors presented above. Both D^* and NEP information

TABLE I
SUMMARY OF THE PERFORMANCE OF CURRENT IR AND TERAHERTZ DETECTORS

Detector type	D* ($cmHz^{1/2}W^{-1}$)	NEP ($W\ Hz^{-1/2}$)	Incident radiation frequency / wavelength	Frame time
Bolometer (VWO) [4], [35]	10^8 - 10^{10} at 77 K [4] 10^6 to 10^8 at 300 K [35]		2 – 40 μm	>1 ms, ultimately limited by the thermal time constant [4], [35]
Photon detector (HgCdTe) [1], [36]	10^{10} at 77 K [1] 10^8 at 300 K [36]		3–30 μm [1] 10.6 μm [36]	< 1 μs, ultimately limited by the device RC time constant [4]
Graphene FET detector [18]		2 x 10^{-7} (single layer) at 300 K 3 x 10^{-8} (double layer) at 300 K	1 THz / 299.8 μm	
Ni-NiO-Ni lumped element MIM rectenna [30]	1.89 x 10^8 at 300 K 8.89 x 10^5 at 300 K		1 THz / 299.8 μm 28 THz / 10.6 μm	
Ni-NiO-Ni travelling wave MIM rectenna [43]	up to 10^9 at 300 K		28 THz / 10.6 μm	
Graphene geometric diode rectenna	10^6 -10^7 at 300 K (device shown) 10^7 -10^8 at 300 K (improved shape)	10^{-8} -10^{-9} at 300 K 10^{-9} -10^{-10} at 300 K	28 THz / 10.6 μm	~ 1 fs, ultimately limited by the rectenna RC time constant

are not available for other types of IR detectors in literature. Therefore we provided both D^* and NEP values for our detectors for convenient comparison. The rectenna detector using a graphene geometric diode provides among the best room temperature IR and terahertz detection performance along with high frame rates.

VII. Night Vision Application Analysis

A major application of the low-cost rectenna IR detectors is in night vision systems, e.g., for use in automobiles. We consider the noise equivalent temperature difference (NETD) to quantify detector performance for night vision applications. NETD is the incident signal temperature required to match the internal noise of the detector, so that the signal-to-noise ratio equals one [8], and corresponds to the lowest temperature difference that can be detected [44]. The requirement for reasonable automotive night vision is to have an IR detector with a NETD value less than 0.3 K [45]. The NETD is calculated as [4]:

$$\mathrm{NETD} = \frac{I_n \sqrt{f_F}}{\beta_{\mathrm{sys}} dP/dT}. \tag{7}$$

In (7), *dP/dT* refers to the thermal variation of the spectral emittance, I_n is the noise current, f_F is the video frame rate, and β_{sys} is the rectenna system responsivity. At a drain source bias of 0 V, the noise current is 12 pA $\mathrm{Hz}^{-1/2}$. For night vision application a video frame rate of 30 Hz is assumed. The geometric diode in Fig. 4, though far from optimal, is used for the following analysis. The device has a diode responsivity of 0.12 A/W at a V_{DS} of 0 V. We use a β_{sys} of 0.06 A/W assuming a 50% antenna absorption efficiency and perfect impedance matching. The differential *dP/dT* can be calculated by subtracting the integral of Planck's law at two temperatures with a temperature difference of 1 K, in a 30 Hz bandwidth over the spectral range of 8 to 14 μm. A typical bolometer night vision system has a pixel pitch of 35 μm [44]. Assuming that the antenna absorbs the radiation with such area, *dP/dT* can be calculated to be 3.2 nW/K [46]. Using the above parameters, the NETD of geometric diodes is ~0.3 K. Using the simulated I(V) and responsivity data, the NETD of geometric diode rectennas can potentially drop to 0.03 K or even lower. This is on the same order of magnitude as the NETD of night vision bolometers, which is ~0.06 K [47]. Photon IR detectors are predicted to have a NETD value of less than 0.1 K at the same frame rate of 30 Hz [36]. Due to the poor coupling efficiency, rectennas using MIM diodes have a much higher NETD value of ~140 K [46]. Thus, geometric diode rectennas are expected to have NETD values that are better than photon IR detectors, and at least as good as those of bolometers, but with the capability of much higher frame rates.

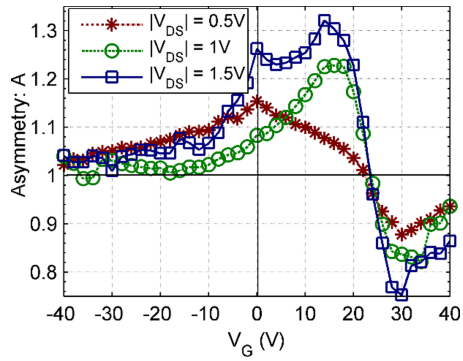

Fig. 11. Measured asymmetry $(A = |I(V_{\mathrm{DS}})/I(-V_{\mathrm{DS}})|)$ as a function of the gate voltage (V_G) for the geometric diode in Fig. 6, at three different drain source voltages: $|V_{\mathrm{DS}}| = 0.5V$, $|V_{\mathrm{DS}}| = 1\mathrm{V}$, and $|V_{\mathrm{DS}}| = 1.5$ V. Diode asymmetry increases with $|V_{\mathrm{DS}}|$. The polarity of the diode switches as the V_G is varied from -40 V to 40 V, due to the change of the charge carrier type from holes to electrons near $V_{\mathrm{CNP}} (= 24V)$. The diode asymmetry ratio reaches its maximum at $V_G = 12$ V and 32 V. This figure is from ref [48].

VIII. Performance Improvement

There are at least four ways to increase the sensitivity of our rectenna detector. The simplest way is to change the diode operating point by applying V_{DS} and V_G to maximize diode *I(V)* asymmetry [48]. Compared to the devices at zero V_{DS}, the geometric effect is greater at higher V_{DS}. We define the diode *I(V)*

asymmetry A to be $|I(V_{\rm DS})/I(-V_{\rm DS})|$. As shown in Fig. 10, the diode asymmetry is highest when $V_{\rm DS}$ equals 1.5 V, compared to that at 1 V and 0.5 V $V_{\rm DS}$. The same drain-source voltage effect can be also seen in Fig 6(b), where applying $V_{\rm DS}$ doubles the β_d from 0.12 A/W at zero bias to ∼0.24 A/W at 1 V bias. A tradeoff of increasing the $V_{\rm DS}$ is that shot noise also increases. For the diode in Fig. 6, the rectenna system performance will first improve with applying $V_{\rm DS}$ and then start to degrade with higher $V_{\rm DS}$. Thus, for geometric diodes, there is a $V_{\rm DS}$ that provides the best system detection performance. Furthermore, increasing the voltage difference ($|V_G - V_{\rm CNP}|$) between V_G and CNP voltage $V_{\rm CNP}$ also leads to greater geometric effect [48]. The charge carrier concentration n of graphene increases and gives a longer MFPL ($\propto \sqrt{n}$) [27]. The *I(V)* asymmetry of the graphene geometric diode in Fig. 11 increases when V_G shifts from 24 to 12 V, and also from 24 to 32 V. However, the diode *I(V)* asymmetry decreases as $|V_G - V_{\rm CNP}|$ increases further, because the current in the device starts to saturate [49]. More details of the graphene gate effect and CNP can be found in reference [48]. Thus, without physically modifying the device, applying $V_{\rm DS}$ and V_G can increase the $\rm D^*$ of the same rectenna device by a factor of two to five, bringing $\rm D^*$ up to close to 10^8 cm $\rm Hz^{1/2}W^{-1}$ and a NEP value $\sim 10^{-10}\rm WHz^{-1/2}$.

The second approach to increasing the diode responsivity is to change the geometric shape of the diodes. We are currently developing geometric diodes with improved geometrical asymmetry. These improved devices in theory can reduce the NEP value to as low as $10^{-11}\rm WHz^{-1/2}$.

Another approach to improve the rectenna detection performance is to improve the quality of graphene and hence the charge MFPL. This can be achieved by improving the fabrication process and reducing chemical contamination of graphene [50]. Boron nitride as substrate has resulted in an improved quality of exfoliated graphene [51], [52].

Last, detection can be improved by changing the antenna. We chose the simplest bowtie antenna due to its ease of fabrication and its polarization-selective absorption efficiency. Many more efficient antenna designs exist [32].

IX. Conclusion

In conclusion, we have developed a new type of IR detector and have demonstrated it for 28 THz radiation, corresponding to a wavelength of 10.6 μm. Rectenna IR detectors incorporating graphene geometric diodes provide optical frequency rectification of 10.6 μm wavelength radiation with both metal and graphene bowtie antennas. The measured short-circuit currents agree with calculate values based on the diode and antenna parameters. The performance of the rectenna IR detector is among the best reported uncooled IR detectors. We calculated the $\rm D^*$ of our detector to be 10^6 cm $\rm Hz^{1/2}W^{-1}$ with a NEP value of 43 nW $\rm Hz^{-1/2}$. Further improvement in the diode and antenna design is expected to increase the detector performance by at least a factor of two. In theory, our rectenna IR detectors can achieve a NEP value as low as $10^{-11}\rm WHz^{-1/2}$.

Acknowledgment

The authors gratefully acknowledge assistance in device preparation from K. Krueger and D. Doroski, and thank B. Pelz for valuable comments on the manuscript. This work was carried out under a contract from Abengoa Solar and the Center for Revolutionary Solar Photoconversion, with initial support from Hub Lab. Device processing was carried out in part at the Colorado Nanofabrication Laboratory, and in part at the Cornell NanoScale Facility, both members of the National Nanotechnology Infrastructure Network, which is supported by the National Science Foundation (Grant ECS-0335765).

References

[1] A. Rogalski, "Infrared detectors: An overview," *Infrared Phys. Technol.*, vol. 43, no. 3–5, pp. 187–210, Jun. 2002.
[2] W. Herschel, "Experiments on the refrangibility of the invisible rays of the sun," *Philosoph. Trans. R. Soc. London*, vol. 90, pp. 284–292, Jan. 1800.
[3] E. Barr, "The infrared pioneers—III. Samuel Pierpont Langley," *Infrared Phys.*, vol. 3, pp. 195–196, Dec. 1963.
[4] A. Rogalski, *Infrared Detectors*, 2nd ed. Boca Raton, FL, USA: CRC Press, 2010.
[5] T. W. Case, "Notes on the change of resistance of certain substances in light," *Phys. Rev.*, vol. 9, no. 4, pp. 305–310, Apr. 1917.
[6] R. J. Cashman, "Film-type infrared photoconductors," *Proc. Inst. Radio Eng.*, vol. 47, no. 9, pp. 1471–1475, 1959.
[7] Z. Zhu, S. Joshi, S. Grover, and G. Moddel, "Graphene geometric diodes for terahertz rectennas," *J. Phys. Appl. Phys.*, vol. 46, no. 18, p. 185101, May 2013.
[8] A. Rogalski, "Infrared detectors: Status and trends," *Prog. Quantum Electron.*, vol. 27, no. 2/3, pp. 59–210, 2003.
[9] S. Grover and G. Moddel, "Applicability of metal/insulator/metal (MIM) diodes to solar rectennas," *IEEE J. Photovoltaics*, vol. 1, no. 1, pp. 78–83, Jul. 2011.
[10] G. Moddel, "Geometric diode, applications and method," U.S. Patent 20 110 017 284, Jul. 17, 2009.
[11] Z. Zhu, S. Grover, K. Krueger, and G. Moddel, "Optical rectenna solar cells using graphene geometric diodes," in *Proc. 37th IEEE Photovoltaic Spec. Conf.*, 2011, pp. 002120–002122.
[12] D. Dragoman and M. Dragoman, "Geometrically induced rectification in two-dimensional ballistic nanodevices," *J. Phys. Appl. Phys.*, vol. 46, no. 5, p. 055306, Feb. 2013.
[13] M. Dragoman, "Graphene nanoelectronics for high-frequency applications," *Proc. SPIE, Nanotechnol. VI*, vol. 8766, pp. 87660C-1–87660C-8, 2013.
[14] A. M. Song, "Electron ratchet effect in semiconductor devices and artificial materials with broken centrosymmetry," *Appl. Phys. A*, vol. 75, no. 2, pp. 229–235, Aug. 2002.
[15] A. H. Castro Neto, F. Guinea, N. M. R. Peres, K. S. Novoselov, and A. K. Geim, "The electronic properties of graphene," *Rev. Mod. Phys.*, vol. 81, no. 1, pp. 109–162, Jan. 2009.
[16] M. Tamagnone, J. S. Gómez-Díaz, J. R. Mosig, and J. Perruisseau-Carrier, "Analysis and design of terahertz antennas based on plasmonic resonant graphene sheets," *J. Appl. Phys.*, vol. 112, no. 11, p. 114915, Dec. 2012.
[17] L. Ju, B. Geng, J. Horng, C. Girit, M. Martin, Z. Hao, H. A. Bechtel, X. Liang, A. Zettl, Y. R. Shen, and F. Wang, "Graphene plasmonics for tunable terahertz metamaterials," *Nat. Nanotechnol.*, vol. 6, no. 10, pp. 630–634, Oct. 2011.
[18] L. Vicarelli, M. S. Vitiello, D. Coquillat, A. Lombardo, A. C. Ferrari, W. Knap, M. Polini, V. Pellegrini, and A. Tredicucci, "Graphene field-effect transistors as room-temperature terahertz detectors," *Nat. Mater.*, vol. 11, no. 10, pp. 865–871, Oct. 2012.
[19] Y. Liu, R. F. Willis, K. V. Emtsev, and T. Seyller, "Plasmon dispersion and damping in electrically isolated two-dimensional charge sheets," *Phys. Rev. B*, vol. 78, no. 20, p. 201403, Nov. 2008.
[20] A. Bostwick, F. Speck, T. Seyller, K. Horn, M. Polini, R. Asgari, A. H. MacDonald, and E. Rotenberg, "Observation of plasmarons in quasi-freestanding doped graphene," *Science*, vol. 328, no. 5981, pp. 999–1002, May 2010.
[21] M. Jablan, H. Buljan, and M. Soljačić, "Plasmonics in graphene at infrared frequencies," *Phys. Rev. B*, vol. 80, no. 24, p. 245435, Dec. 2009.
[22] C.-H. Park, F. Giustino, M. L. Cohen, and S. G. Louie, "Electron-phonon interactions in graphene, bilayer graphene, and graphite," *Nano Lett.*, vol. 8, no. 12, pp. 4229–4233, Dec. 2008.

[23] N. W. Ashcroft and N. D. Mermin, *Solid State Physics*. Fort Worth, TX, USA: Harcourt College, 1976.
[24] F. Xia, T. Mueller, Y. Lin, A. Valdes-Garcia, and P. Avouris, "Ultrafast graphene photodetector," *Nat. Nanotechnol.*, vol. 4, no. 12, pp. 839–843, Dec. 2009.
[25] K. I. Bolotin, K. J. Sikes, Z. Jiang, M. Klima, G. Fudenberg, J. Hone, P. Kim, and H. L. Stormer, "Ultrahigh electron mobility in suspended graphene," *Solid State Commun.*, vol. 146, no. 9/10, pp. 351–355, Jun. 2008.
[26] A. S. Mayorov, R. V. Gorbachev, S. V. Morozov, L. Britnell, R. Jalil, L. A. Ponomarenko, P. Blake, K. S. Novoselov, K. Watanabe, T. Taniguchi, and A. K. Geim, "Micrometer-scale ballistic transport in encapsulated graphene at room temperature," *Nano Lett.*, vol. 11, no. 6, pp. 2396–2399, Jun. 2011.
[27] O. M. Nayfeh, "Radiofrequency transistors using chemical-vapor-deposited monolayer graphene: Performance, doping, and transport effects," *IEEE Trans. Electron. Devices*, vol. 58, no. 9, pp. 2847–2853, Sep. 2011.
[28] M. D. Weiss, B. J. Eliasson, and G. Moddel, "Terahertz device integrated antenna for use in resonant and non-resonant modes and method," U.S. Patent 6 835 949, B228 Dec. 2004.
[29] P. Joshi, H. E. Romero, A. T. Neal, V. K. Toutam, and S. A. Tadigadapa, "Intrinsic doping and gate hysteresis in graphene field effect devices fabricated on SiO2 substrates," *J. Phys. Condens. Matter*, vol. 22, no. 33, p. 334214, Aug. 2010.
[30] Z. Zhu, S. Joshi, S. Grover, and G. Moddel, "Geometric diodes for optical rectennas," in *Rectenna Solar Cells* New York, NY, USA Springer, 2013, pp. 209–227.
[31] J. R. Williams, L. DiCarlo, and C. M. Marcus, "Quantum hall effect in a gate-controlled p-n junction of graphene," *Science*, vol. 317, no. 5838, pp. 638–641, Aug. 2007.
[32] F. J. González and G. D. Boreman, "Comparison of dipole, bowtie, spiral, and log-periodic IR antennas," *Infrared Phys. Technol.*, vol. 46, no. 5, pp. 418–428, Jun. 2005.
[33] I. Kocakarin and K. Yegin, "Glass superstrate nanoantennas for infrared energy harvesting applications," *Int. J. Antennas Propag.*, vol. 2013, Mar. 2013.
[34] P. L. Richards, "Bolometers for infrared and millimeter waves," *J. Appl. Phys.*, vol. 76, no. 1, pp. 1–24, Jul. 1994.
[35] N. Chi-Anh, H.-J. Shin, K. Kim, Y.-H. Han, and S. Moon, "Characterization of uncooled bolometer with vanadium tungsten oxide infrared active layer," *Sens. Actuators Phys.*, vol. 123–124, pp. 87–91, Sep. 2005.
[36] J. Piotrowski, M. Grudzien, Z. Nowak, Z. Orman, J. Pawluczyk, M. Romanis, and W. Gawron, "Uncooled photovoltaic Hg1-xCdxTe LWIR detectors," vol. 4130, pp. 175–184, 2000.
[37] M. Razeghi, "Current status and future trends of infrared detectors," *Opto-Electron. Rev.*, vol. 6, no. 3, pp. 155–194, 1998.
[38] C. Fumeaux, W. Herrmann, F. K. Kneubühl, and H. Rothuizen, "Nanometer thin-film Ni–NiO–Ni diodes for detection and mixing of 30 THz radiation," *Infrared Phys. Technol.*, vol. 39, no. 3, pp. 123–183, Apr. 1998.
[39] I. Codreanu, F. J. Gonzalez, and G. D. Boreman, "Detection mechanisms in microstrip dipole antenna-coupled infrared detectors," *Infrared Phys. Technol.*, vol. 44, no. 3, pp. 155–163, Jun. 2003.
[40] A. Sanchez, C. F. Davis, K. C. Liu, and A. Javan, "The MOM tunneling diode: Theoretical estimate of its performance at microwave and infrared frequencies," *J. Appl. Phys.*, vol. 49, no. 10, pp. 5270–5277, 1978.
[41] S. Y. Wang, T. Izawa, and T. K. Gustafson, "Coupling characteristics of thin-film metal-oxide-metal diodes at 10.6 μ," *Appl. Phys. Lett.*, vol. 27, no. 9, pp. 481–483, 1975.
[42] M. J. Estes and G. Moddel, "Surface plasmon devices," U.S. Patent 701 018 307, Mar. 2006.
[43] S. Grover, O. Dmitriyeva, M. J. Estes, and G. Moddel, "Traveling-wave metal/insulator/metal diodes for improved infrared bandwidth and efficiency of antenna-coupled rectifiers," *IEEE Trans. Nanotechnol.*, vol. 9, no. 6, pp. 716–722, Nov. 2010.
[44] G. Meyer, "Far infrared imaging sensor for mass production of night vision and pedestrian detection systems," in *Advanced Microsystems for Automotive Applications 2012: Smart Systems for Safe, Sustainable and Networked Vehicles*. Berlin, Germany: Springer, 2012.
[45] ADOSE, "*Reliable Application Specific Detection Of Road Users With Vehicle On-Board Sensors*, Mar. 10, 2008.
[46] S. Grover, "Diodes for optical rectennas," Ph.D. dissertation, Univ. Colorado Boulder, Boulder, CO, USA, 2011.
[47] J. J. Yon, E. Mottin, L. Biancardini, L. Letellier, and J. L. Tissot, "Infrared microbolometer sensors and their application in automotive safety," in *Advanced Microsystems for Automotive Applications*, D. J. Valldorf and D. W. Gessner, Eds. Heidelberg, Germany: Springer, 2003, pp. 137–157.
[48] G. Moddel, Z. Zhu, S. Grover, and S. Joshi, "Ultrahigh speed graphene diode with reversible polarity," *Solid State Commun.*, vol. 152, no. 19, pp. 1842–1845, Oct. 2012.
[49] V. E. Dorgan, M.-H. Bae, and E. Pop, "Mobility and saturation velocity in graphene on SiO2," *Appl. Phys. Lett.*, vol. 97, no. 8, p. 082112, Aug. 2010.
[50] J. Fan, J. M. Michalik, L. Casado, S. Roddaro, M. R. Ibarra, and J. M. De Teresa, "Investigation of the influence on graphene by using electron-beam and photo-lithography," *Solid State Commun.*, vol. 151, no. 21, pp. 1574–1578, Nov. 2011.
[51] Z. Liu, L. Ma, G. Shi, W. Zhou, Y. Gong, S. Lei, X. Yang, J. Zhang, J. Yu, K. P. Hackenberg, A. Babakhani, J.-C. Idrobo, R. Vajtai, J. Lou, and P. M. Ajayan, "In-plane heterostructures of graphene and hexagonal boron nitride with controlled domain sizes," *Nat. Nanotechnol.*, vol. 8, no. 2, pp. 119–124, Feb. 2013.
[52] M. P. Levendorf, C.-J. Kim, L. Brown, P. Y. Huang, R. W. Havener, D. A. Muller, and J. Park, "Graphene and boron nitride lateral heterostructures for atomically thin circuitry," *Nature*, vol. 488, no. 7413, pp. 627–632, Aug. 2012.

Zixu Zhu (S'08) was born in Tianjin, China. He received the Bachelor's degree in electrical engineering from Brigham Young University, Provo, UT, USA, in 2008, and the Master's degree the from University of Colorado (Boulder), Boulder, CO, USA, in 2011. He is currently working toward the Ph.D. degree in the Quantum Engineering Laboratory, University of Colorado (Boulder).

He has extensive hands-on nanofabrication process development experience in many nanofabrication facilities across the U.S., including: Cornell Nanofabrication Facility, UCSB Nanofabrication Facility, Colorado Nanofabrication Lab, University of Colorado Nanomaterials Characterization Facility, JILA Keck lab, and Brigham Young University Integrated Microfabrication Lab. His research interests include nanofabrication process development, ultrahigh speed graphene devices, photovoltaic technology, metal/insulator/metal tunnel diodes, and terahertz detectors.

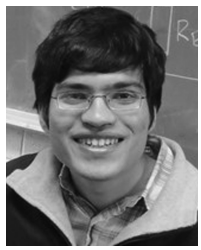

Saumil Joshi (S'09) received the Bachelor of Engineering degree from the University of Delhi, Delhi, India, in 2009. He is currently working toward the Ph.D. degree at the Department of Electrical, Computer, and Energy Engineering, University of Colorado, Boulder, CO, USA.

As a graduate student, he is working on the development, analysis, and characterization of high-speed diodes and rectennas. His research interests include electron transport at the nanoscale, rectennas for energy harvesting, and optical detection.

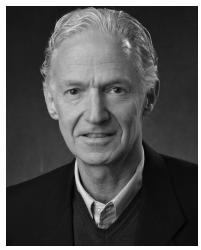

Garret Moddel (SM'93) was born in Dublin, Ireland. He received the B.S.E.E. degree from Stanford University, Stanford, CA, USA, in 1976, and the M.S. and Ph.D. degrees in applied physics from Harvard University, Cambridge, MA, USA, in 1976 and 1978, respectively.

After graduation, he became a Founding Employee at SERA Solar Corp., a Silicon Valley photovoltaics start-up company. He joined the University of Colorado, Boulder, CO, USA, in 1985, where he is a Professor of Electrical, Computer, and Energy Engineering. At the CU, he has developed new thin-film optoelectronic materials and devices. Currently, his research group works in quantum engineering of new thin-film metal devices for energy conversion and detection. He was the Founding President and CEO of Phiar Corporation, a venture-capital-backed high-tech start-up developing ultrahigh-speed metal-insulator electronics.

Dr. Moddel was named the first CU Inventor of the Year in the Physical Sciences in 2002, and is a Fellow of the Optical Society of America.